



Available online at www.sciencedirect.com



ScienceDirect

Reliability Engineering and System Safety 00 (2014) 1–17

Reliability
Engineer-
ing &
System
Safety

Coupling mode-destination accessibility with seismic risk assessment to identify at-risk communities

Mahalia Miller^{a,1,*}, Jack W. Baker^a

^aDepartment of Civil and Environmental Engineering, Stanford University, 439 Panama Mall, MC:3037, Stanford, CA 94305, United States

Abstract

In this paper, we develop a framework for coupling mode-destination accessibility with quantitative seismic risk assessment to identify communities at high risk for travel disruptions after an earthquake. Mode-destination accessibility measures the ability of people to reach destinations they desire; it is calculated as the log value of the sum of a function of the utilities of each destination over all possible destinations and travel modes, where the utility decreases if getting to that destination is more costly or time-intensive. We use a probabilistic seismic risk assessment procedure, including a stochastic set of earthquake events, ground-motion intensity maps, damage maps, and realizations of traffic and accessibility impacts. For a case study of the San Francisco Bay Area, we couple our seismic risk framework with a practical activity-based traffic model. As a result, we quantify accessibility risk probabilistically by community and household type. We find that accessibility varies more strongly as a function of travelers' geographic location than as a function of their income class, and we identify particularly at-risk communities. We also observe that communities more conducive to local trips by foot or bike are predicted to be less impacted by losses in accessibility. This work shows the potential to link quantitative risk assessment methodologies with high-resolution travel models used by transportation planners. Quantitative risk metrics of this type should have great utility for planners working to reduce risk to a region's infrastructure systems.

© 2014 Published by Elsevier Ltd.

Keywords: Infrastructure, Risk, Earthquakes, Transportation Network, Accessibility

1. Introduction

Seismic risk assessment in earthquake engineering tends to focus on buildings, bridges, and the performance of infrastructure systems. For measuring the performance of transportation systems, researchers typically use engineering-based metrics such as the post-earthquake connectivity loss, which quantifies the decrease in the number of origins or generators connected to a destination node [e.g., 1], or the post-earthquake travel distance between two locations of interest [e.g., 2]. These frameworks have provided insight into seismic vulnerability and possible risk mitigation, but do not directly quantify ramifications for people.

In the field of vulnerability sciences, researchers have long stressed the importance of the impact on human welfare from earthquakes. For example, Bolin and Stanford write that, “‘Natural’ disasters have more to do with the social,

*Corresponding author: Phone: +1-617-692-0574

Email addresses: mahalia@alum.mit.edu (Mahalia Miller), bakerjw@stanford.edu (Jack W. Baker)

URL: web.stanford.edu/~bakerjw/ (Jack W. Baker)

¹Present address: Google Inc., 345 Spear St., Floor 4, San Francisco, CA 94114, United States

political, and economic aspects than they do with the environmental hazards that trigger them. Disasters occur at the interface of vulnerable people and hazardous environments” [3]. A recent World Bank and United Nations report echoed this idea that the effects on human welfare turn natural hazards into disasters [4]. Historical events demonstrate the complex social effects of earthquakes. For example, on one hand the 1994 Northridge earthquake caused major damage to nine bridges, which, while significant, represented only 0.5% of the bridges estimated by Caltrans to have experienced significant shaking [5]. On the other hand, over half of businesses reported closing after the earthquake, with 56% citing the “inability of employees to get to work” as a reason [6]. Furthermore, the total economic cost of transport-related interruptions (“commuting, inhibited customer access, and shipping and supply disruptions”) from this earthquake is estimated at 2.16 billion USD (2014) [7], using the consumer price index to account for inflation.

Some researchers have measured the impact of earthquakes on transportation infrastructure using the cumulative extra time needed for travel due to damage, sometimes called travel time delay [e.g., 8, 9]. This performance measure captures basic re-routing due to road closures and identifies roads more likely to be congested. Travel time approximately measures impact on people, but does not capture the fact that some destinations and trips have higher value than others. It also focuses on aggregate regional effects rather than individual communities and demographic groups. Others have considered the qualitative criteria-based metric “disruption index” [10], but this does not provide a quantitative link between physical damage to infrastructure and resulting human ramifications. Other work has looked at resiliency, but defined it in pure engineering terms, such as percentage of a road network that is functional [11]. Outside of transportation systems, some researchers have investigated the interplay between earthquake damage to the electric power and wastewater networks, and the usability of houses and other buildings [12].

In contrast to the work on transportation-related seismic risk, urban planning has a long tradition of studying the impact on people of events and policy [13]. Accessibility is one popular metric to measure the impact of different transportation network scenarios, and it measures how easily people can get to desirable destinations, which is one measure of social impact [14]. Within urban planning, accessibility has been measured in many ways, including individual accessibility, economic benefits of accessibility, and mode-destination accessibility [15]. The mode-destination accessibility is computed by taking the log value of the sum of a function of the utilities of each destination over all possible destinations and travel modes, where the utility decreases if getting to that destination is more costly or time-intensive [16]. This choice of accessibility definition is particularly useful for quantifying the impacts of disasters such as earthquakes, because certain destinations might be more critical for people in certain locations or from certain socio-economic groups. However, this accessibility measure has not previously been linked to risk assessment. In addition, the majority of work to date assumes that travel demand and mode choice will remain unchanged after a future earthquake, which historical data suggests is not the case [7]. A first step towards considering variable demand is work in the literature that varies demand by applying a constant multiplicative factor on all pre-earthquake travel demand [8], but again this approach lacks any resolution at the geographic or socio-economic level.

In this paper, we develop a framework for coupling mode-destination accessibility with a quantitative seismic-risk assessment to identify at-risk populations and measure the accompanying impacts on human welfare. We illustrate our approach with a case study of the San Francisco Bay Area transportation network, including highways, local roads, and public transportation lines. This study analyzes a set of forty hazard-consistent earthquake scenarios, ground-motion intensity maps, and damage maps, as introduced in [17, 18]. For each of these damage maps, we model damage with an agent-based transportation model used by the local transportation authorities that considers the impacts of damage to bridges, roads, and transit lines, and captures variable user demand. Then, with this model, we estimate losses in accessibility for 12 socio-economic groups and for a number of communities within the study region.

2. Case study: San Francisco Bay Area

We consider the San Francisco Bay Area to illustrate our approach (Figure 1). This seismically active area follows a polycentric metropolitan form, with San Francisco as the primary center and other jobs concentrated in suburban centers such as San Jose [19]. The region has a wide array of trip patterns for mandatory and non-mandatory trips. Furthermore, trip times and routes vary greatly depending on travel preferences and workplace locations [19]. Thus, there may be noticeable disparities among households in the risk of travel-related impacts due to earthquakes.

This analysis considers the complex web of roads and transit networks of the case study area. The roads are modeled by a directed graph $G = (V, E)$, where V is a finite set of vertices representing intersections, and the set

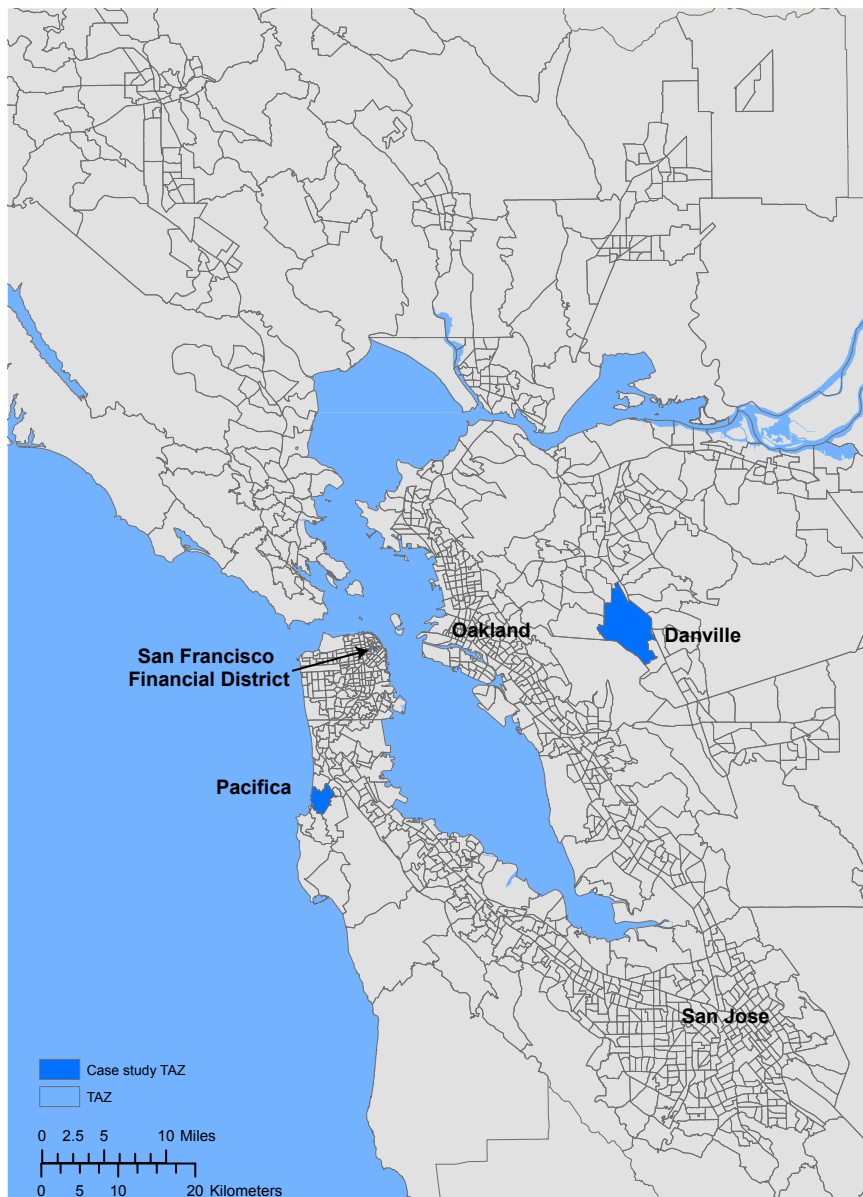


Figure 1. Travel analysis zones (TAZs) in the San Francisco Bay Area. Shading indicates the Danville, Pacifica and San Francisco Financial District TAZs that are considered in more detail below.

E, whose elements are edges representing road links, is a binary relation on *V*. In this model, ($|V|, |E|$) = (11,921, 32,858) including centroidal links and ($|V|, |E|$) = (9,635, 24,404) without. Centroidal links do not correspond to particular physical roads but instead capture flows of people from outside the study area or from some minor local roads. Forty-three transit networks such as bus, light rail and ferry systems are also modeled. We model potential damage to 1743 highway bridges impacting the road and some transit networks, and 1409 structures impacting the rapid transit network, BART. Details of the seismic risk calculations for this network are provided in the following subsections.

67 2.1. Ground-motion intensity maps

68 2.1.1. Theory

69 We now describe how to produce a set of maps with ground-motion intensity realizations at each location of interest, and corresponding occurrence rates that reasonably capture the joint distribution of the ground-motion intensity 70 at all locations of interest throughout the region [e.g., 20]. First, we generate *Q* earthquake scenarios from a seismic 71 source model, which specifies the rates at which earthquakes of various magnitudes, locations, and faulting types will 72 occur. This set of earthquake scenarios is comparable to a stochastic event catalogue in the insurance industry.

73 Second, for each earthquake scenario in the seismic source model, we use an empirical ground-motion prediction 74 equation (GMPE) to predict the log mean and standard deviation of a ground motion intensity measure at each location 75 of interest. Then, for each of the *Q* earthquake scenarios, we sample *b* realizations of spatially correlated ground- 76 motion intensity residual terms. The total log ground-motion intensity (*Y*) for a given realization is computed as

$$\ln Y_{ij} = \overline{\ln Y(M_j, R_{ij}, V_{s30,i}, \dots)} + \sigma_{iq}\epsilon_{ij} + \tau_j\eta_j \quad (1)$$

77 where $\overline{\ln Y(M_j, R_{ij}, V_{s30,i}, \dots)}$ is the predicted mean log ground motion intensity at location index *i*, given an 78 earthquake of magnitude *M_j* at a distance of *R_{ij}*, observed at a site with average shear wave velocity down to 30m of *V_{s30,i}*. Variability in ground motion intensity about this mean value is represented by σ_{iq} and τ_j , the within- and between- 79 event standard deviations, respectively, for earthquake scenarios at the index *q* = 1, ..., *Q*. The index *j* indicates the 80 ground-motion intensity map (*j* = 1, ..., *m* where *m* = *Q* × *b*), ϵ_{ij} is a normalized within-event residual representing 81 location-to-location variability and η_j is the normalized between-event residual. Both ϵ_{ij} and η_j are normal random 82 variables with zero mean and unit standard deviation. The vector of ϵ_{ij} has a multivariate normal distribution and η_j 83 is univariate.

84 The result is a set of *m* ground-motion intensity maps (e.g., Figure 2a). Since we simulate an equal number (*b*) 85 of ground-motion intensity maps per earthquake scenario, the annual rate of occurrence for the *jth* ground-motion 86 intensity map is the original rate of occurrence of the earthquake scenario, divided by *b*. We denote the occurrence 87 rate of the *jth* ground-motion intensity map as *w_j*.

88 2.1.2. Implementation

89 To generate a stochastic catalog of ground-motion intensity maps, we use the OpenSHA Event Set Calculator [21]. This 90 software outputs the mean, $\ln Y_{ij}$, and standard deviation values, σ_{ij} and τ_j , for all locations of interest for a 91 specified seismic source model and ground-motion prediction equation, which are needed inputs for Equation 1. The 92 intensity measure is the 5%-damped pseudo absolute spectral acceleration (*Sa*) at a period *T* = 1s, which is the 93 required input to the fragility functions below. This spectral acceleration value represents the maximum acceleration 94 over time that a linear oscillator with 5% damping and a period of 1s will experience from a given ground motion. 95 We calculate these values at the location of each component (i.e., bridges and other structures). Using one ground- 96 motion intensity measure per component is a common simplification that facilitates the use of fragility functions to 97 easily predict damage to a given type of structure [e.g., 9, 22]. We use the UCERF2 seismic source model to specify 98 occurrence rates of potential earthquakes in the region [23], the Wald and Allen topographic slope model to infer *V_{s30,i}* 99 at each location [24], the Boore and Atkinson [25] ground-motion prediction equation and the Jayaram and Baker 100 model [26] for spatial correlation of ϵ_{ij} values.

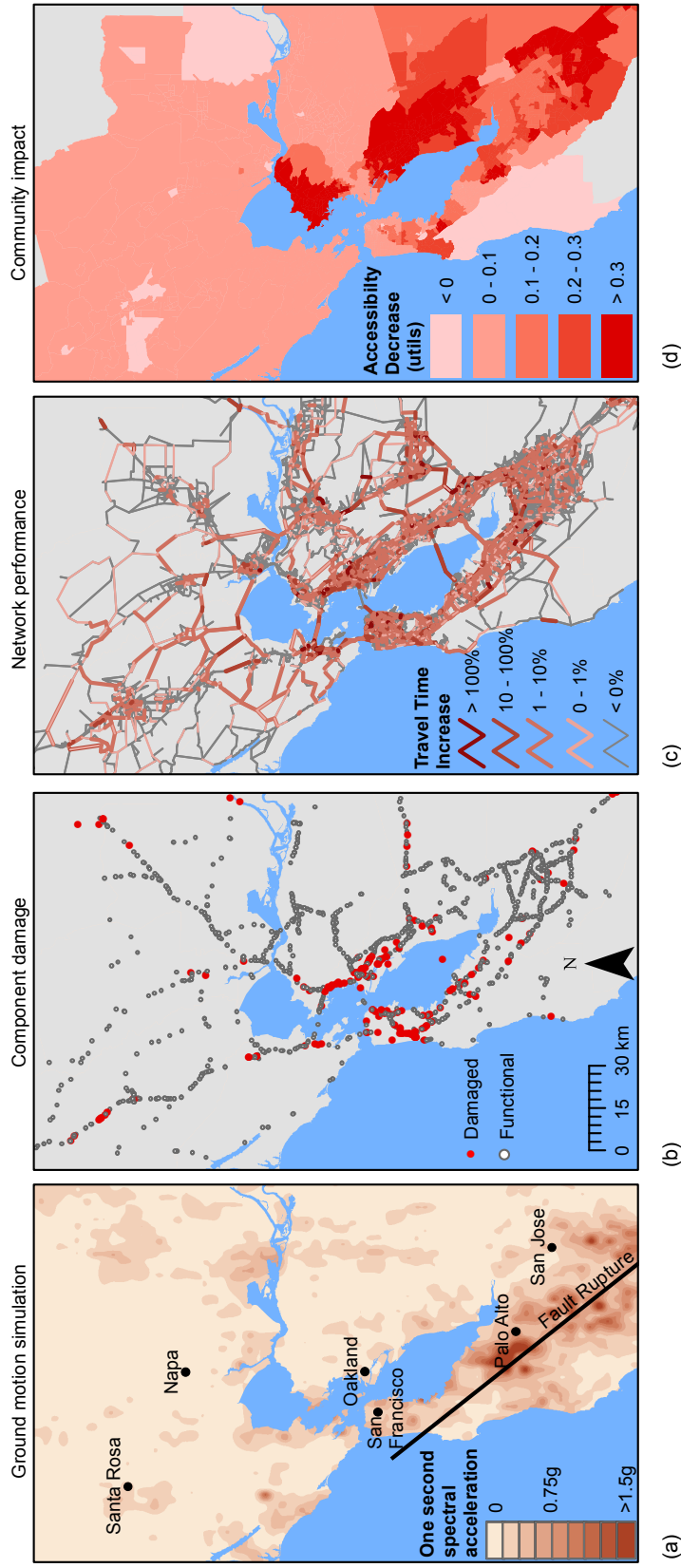


Figure 2. Illustration of the risk framework for one earthquake event including a) earthquake rupture and one-second spectral acceleration (ground motion intensity) map, b) bridge (component) damage map, c) map of travel time increase (network-performance measure) values and d) map of average accessibility decrease per travel analysis zone.

103 **2.2. Damage maps**

104 **2.2.1. Theory**

105 The link between ground-motion intensity and damage to network components is provided by fragility functions.
 106 Fragility functions express the probability $P(DS_i \geq ds_s | Y_{ij} = y)$, where DS_i is a discrete random variable representing
 107 the damage state for the i^{th} component and ds_s is a damage state threshold of interest. The damage state is conditioned
 108 on the ground motion intensity Y_{ij} having value y . We assume one component per location, and so identify both com-
 109 ponents and locations via the index i . Researchers have calibrated fragility functions using historical post-earthquake
 110 data [e.g., 27], experimental and analytical results [e.g., 28], hybrid approaches, and expert opinion.

111 By sampling a damage state for each component, with probabilities obtained from the fragility functions given
 112 the ground-motion intensity, we produce a damage map (e.g., Figure 2b). The sampling process can be repeated to
 113 simulate multiple damage maps per ground-motion intensity map. For example, if c damage maps are sampled per
 114 ground-motion intensity map, the occurrence rates associated with the j^{th} damage map should be adjusted accordingly
 115 to $w_{j'} = w_j/c$, and $j' = 1, \dots, J$.

116 *Functional percentage* relationships link the component damage to the functionality of network elements. For
 117 example, in a road network, when a bridge collapses, the traffic flow capacity of the road it carries and it crosses are
 118 reduced to zero. These relationships are typically derived from a combination of observation and expert opinion, often
 119 due to data scarcity [29]. Furthermore, the relationships are typically deterministic for a certain component damage
 120 state and restoration time [29]. Thus, in this paper, each damage map corresponds to a functionality state for every
 121 element of the network.

122 **2.2.2. Implementation**

123 *Component damage.* We use fragility functions of the following form to provide the link between ground-motion
 124 shaking and component damage:

$$P(DS_i \geq ds_s | Y_{ij} = y) = \Phi\left(\frac{\ln y - \lambda_{s,i}}{\xi_{s,i}}\right), \quad (2)$$

125 where Φ is the standard normal cumulative distribution function, $\lambda_{s,i}$ and $\xi_{s,i}$ are respectively the mean and standard
 126 deviation of the $\ln Y_{ij}$ value necessary to cause the s^{th} damage state to occur or be exceeded for the i^{th} component, and
 127 the other variables are defined above.

128 The California Department of Transportation (Caltrans) provided the fragility function values $\lambda_{s,i}$ and $\xi_{s,i}$ used
 129 for road bridges in this study [30]. The $\lambda_{s,i}$ values are based on bridge characteristics including number of spans and
 130 age [27], and the $\xi_{s,i}$ values are constant for all bridges. The BART seismic safety group provided the fragility function
 131 values $\lambda_{s,i}$ and $\xi_{s,i}$ used in this study for the BART-related components [31]; data is available for the aerial structures,
 132 primarily in the East Bay, but not tunnels. The BART fragility function values correspond to the safety performance
 133 goals under the recent retrofit program, and both the $\lambda_{s,i}$ and $\xi_{s,i}$ vary depending upon the structure's characteristics.
 134 Both sets of fragility functions are based on the assumption that damage can be reasonably accurately estimated by
 135 the ground motion intensity at each site independently, and that the damage state can be reasonably estimated by
 136 an analytical model considering a single ground-motion intensity measure. In addition, the fragility curves do not
 137 directly consider the effects of degradation. Current work is ongoing to refine these assumptions [e.g., 28, 32, 33]. Per
 138 ground-motion intensity map, we sample one damage map (e.g., Figure 2b), which has a realization of the component
 139 damage state at each component location according to the fragility function (eq. 2).

140 *Transit network damage.* Each of the 43 transit systems we considered will function differently when damaged.
 141 Because the Caltrain rail system consists of a single set of shared tracks, managers suggested that the system would
 142 either be fully operational, or not at all if even one segment of the system was non-operational. Similarly, managers
 143 suggested modeling the VTA system as either fully or not at all functional. Depending on where the BART train
 144 cars are when the earthquake strikes, the agency could accommodate different emergency plans. However, BART
 145 representatives suggested that if any part of a route is damaged, the entire corresponding route would not be operational
 146 (but other routes on different tracks might be still operational). In other words, each BART route as well as the
 147 Caltrain and VTA routes are weakest-link systems, so the failure of a single component will cause the route to be
 148 non-operational. We modeled the ferry systems as fully functioning for all earthquake events. For all earthquake
 149 events including the baseline, trans-bay and cross-county bus lines were discontinued, but main lines in urban areas

as well as other local bus networks were maintained per recommendations from the MTC (though they face the same delays due to post-disaster traffic congestion as car travelers).

Road network damage. The damage state of each Caltrans bridge maps directly to the traffic capacity on associated road segments. Based on discussions with Caltrans, we consider travel conditions one week after an earthquake, since it is a critical period for decision making (for example, bridges would have been inspected and surface damage repaired, but major reconstruction would not have yet begun). At this point in time, the components are assumed to have either zero or full traffic capacity [29]. We can thus summarize the component damage using two damage states, $ds_{damaged}$ (corresponding to HAZUS extensive or complete damage states) and $ds_{functional}$ (none, slight, or moderate damage states) [29]. Thus, the functional percentage relationship assigns zero traffic capacity on road segments that have at least one component in the $ds_{damaged}$ damage state, and full traffic capacity otherwise.

2.3. Network performance

2.3.1. Theory

The final step for the event-based risk analysis is to evaluate the network performance measure, X . For this application, we consider mode-destination accessibility change [e.g., 15, 34, 35] (e.g., Figure 2d). Mode-destination accessibility, hereafter referred to as accessibility, measures the distribution of travel destination opportunities weighted by the composite utility of all modes of travel to those destinations (i.e., the ease of someone getting to different destinations weighted by how desirable those destinations are) [16, 14]. The utility function for the mode-destination choice may be estimated using a multinomial random utility model where the logsum represents the accessibility value [36, 16, 14]. Namely, accessibility for a particular agent a is

$$Acc_a = \ln \left[\sum_{v \in C_a} \exp(V_{a(c)}) \right] \quad (3)$$

where $V_{a(c)}$ is the utility of the c^{th} choice for the a^{th} person, and C_a is the choice set for the a^{th} person [16]. Choices refer to travel destinations and the mode of travel (driving, walking, bus, etc.). The units are a dimensionless quantity, *utils*, but can be converted into equivalent time and dollar amounts using *compensating variation* for cost-benefit studies. For the case study, 1 *util* equals the value of 75 minutes or \$20 per person per day [14, 37, 38, 39]. With nearly 7 million people in the study region, even small changes in average *utils* lead to large economic impacts. Since accessibility measures how easily people can get to the destinations they desire, it is a measure of human welfare [e.g., 14].

Once the accessibility network performance measure is computed for each damage map, we aim to estimate the exceedance rate of different levels of performance. The annual rate, λ , of exceeding some threshold of network performance is estimated by summing the occurrence rates of all damage maps in which the performance measure exceeds the threshold:

$$\lambda_{X \geq x} = \sum_{j'=1}^J w_{j'} \mathbb{I}(X_{j'} \geq x) \quad (4)$$

where x is an accessibility value threshold of interest and $X_{j'}$ is the accessibility value realization for the j'^{th} damage map. The variable $w_{j'}$ is the occurrence rate of the j'^{th} damage map. The indicator function \mathbb{I} evaluates to 1 if the argument, $X_{j'} \geq x$, is true, and 0 otherwise. By evaluating λ at different threshold values, we derive an exceedance curve.

2.3.2. Implementation

We compute accessibility using *Travel Model One* (version 0.3), an activity-based model used by the Metropolitan Transportation Commission (MTC), the local metropolitan planning organization (MPO) [40]. It represents the full road network as well as the public transit networks, biking, and walking. Travel demand data consists of the locations of different households in the case study area, their destination preferences and utilities, their number of vehicles, and their income and other demographic data [40, 38, 41]. This data was collected by the MTC from surveys and census information. We assume that the distributions of travel preferences do not change after an earthquake, although

Table 1. Income class definitions for the case study region, as defined by the local planning organization, the MTC [38] and also translated to current 2014 USD using the consumer price index.

Income class	Income range, 1989 USD	Income range, 2014 USD
Low	< \$25,000	< \$47,334
Medium	\$25,000 - \$45,000	\$47,334 - \$85,202
High	\$45,000 - \$75,000	\$85,202 - \$142,004
Very high	> \$75,000	> \$142,004

191 the actual destinations and trips will vary as people choose to forgo trips due to network disruption. The result
 192 is a variable-travel-demand model. This model uses a combination of Java code called CT-RAMP [42], and the
 193 Citilabs Cube Voyager and Cube Cluster transportation planning software [40]. The software takes 6+ hours on a
 194 high-performance computing platform to analyze a given network state, including reaching equilibrium on users trip
 195 choices and preferred travel modes and routes.

196 Given the computational cost of analyzing the network, analyzing thousands of scenarios with a crude Monte Carlo
 197 approach is not feasible. This analysis uses an improved sampling strategy to select damaged networks for analysis,
 198 and considers 40 sets of ground-motion intensity maps, damage maps, accessibility performance measure realizations,
 199 and corresponding annual rates of occurrence. The 40 realizations were selected (and their occurrence rates adjusted
 200 appropriately) using an optimization procedure to ensure that the selected scenarios were consistent with the larger
 201 original set of simulations, in terms of the probability distributions of ground motion intensity at individual sites,
 202 and other parameters that ensured reasonableness of the distributions of network damage. In this sense, the selected
 203 simulations are a “hazard consistent” representation of the distribution of future earthquake impacts that could be
 204 experienced in the region. Readers are referred to [17] for more details about this set of events and computing mode-
 205 destination accessibility using this model.

206 3. Results and discussion

207 3.1. Region-wide results

208 In this section, we analyze region-wide trends in accessibility losses for the case study area. We first analyze
 209 each of the 12 socio-economic groups used in practice for the case study region [38]. These socio-economic groups
 210 correspond to all combinations of four income classes (Table 1), and three classes of automobile availability in the
 211 household (zero automobiles, fewer automobiles than household members that work, as many or more automobiles
 212 than household members that work). Each data point for analysis represents a trip by a person of a household from
 213 one of these segments, who is modeled as an agent in the transportation model. Expected losses are computed by
 214 taking an average of the accessibility losses for people within a given group and region for each earthquake event,
 215 weighted by the events’ corresponding occurrence rates. Expected losses for people from each of the 12 groups and
 216 1454 TAZs are shown in Figure 3.

217 In addition to looking at average accessibility loss, we can compute an accessibility exceedance curve for a given
 218 group or region. By using equation 4 to compute exceedance rates for multiple accessibility loss thresholds, we can
 219 produce results like those in Figure 4. These curves show, for a given group, the annual rate with which a given
 220 accessibility decrease will be observed (when considering random future occurrences of earthquakes and damage).
 221 Several observations can be made from these results.

222 First, a higher ratio of cars to the number of people who work in a household corresponds to a higher expected
 223 decreases in accessibility (as seen by looking across a column in Figure 3). Households with more cars tend to
 224 take longer trips, and there is a relationship between needing to travel longer distances and needing an extra car
 225 in a household. But there is only a weak trend between average trip length for a TAZ and the predicted impact on
 226 accessibility (Figure 5). Instead, we hypothesize that there are other latent variables correlated with both car ownership
 227 and accessibility risk (such as geographic location). In Section 3.5, we will further explore the relationship between
 228 the percentage of car-based trips and accessibility risk.

229 Second, controlling for car ownership, we see a fairly consistent distribution of risk across income classes. For
 230 example, looking at households with fewer workers than cars (the middle column of Figure 3), the variation from

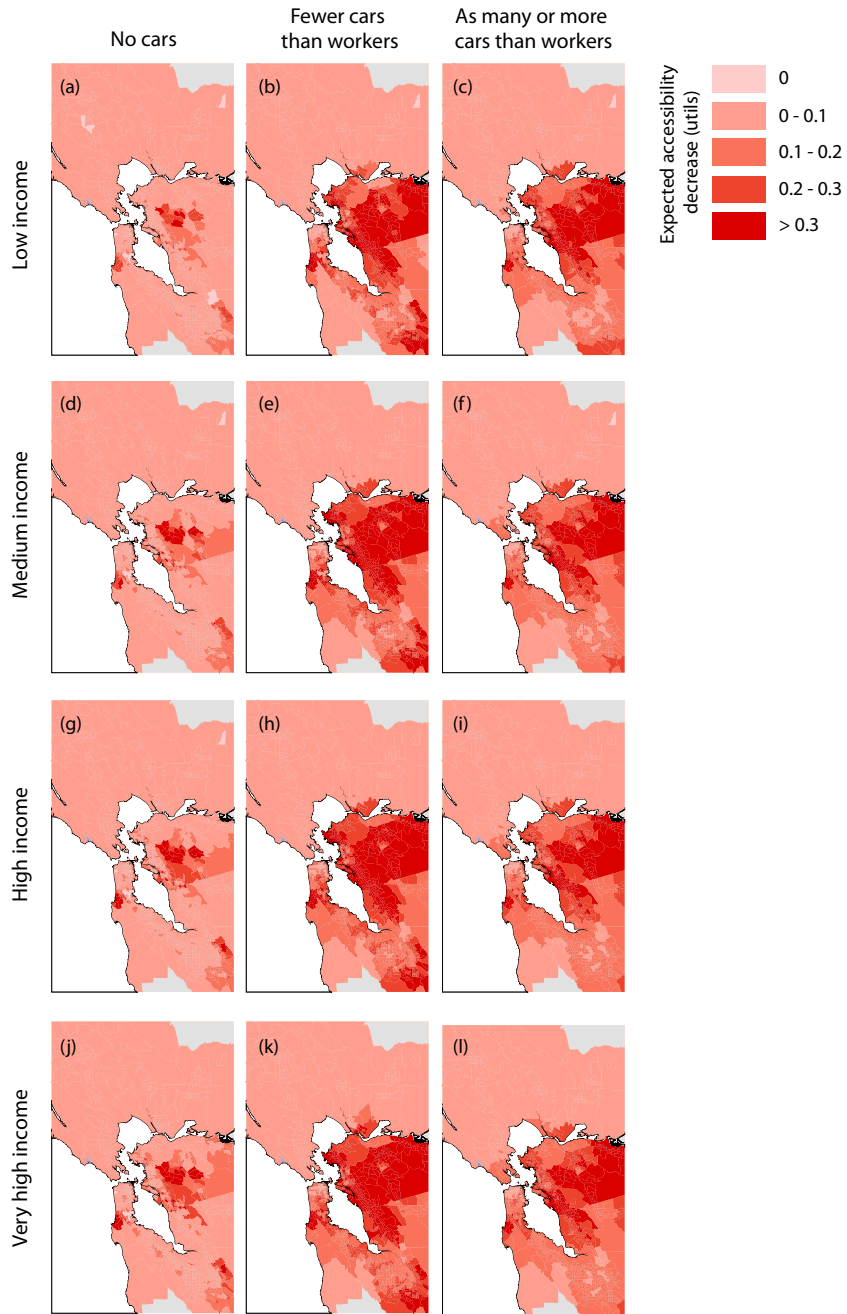


Figure 3. Expected changes in accessibility per person per day for each combination of income class and car ownership group. The darker the color, the greater the losses in accessibility. Each row of figures corresponds to an income class and each column corresponds to a class of car ownership.

TAZ to TAZ is much greater than the difference across income segments. Similarly, while trip lengths are slightly longer for higher income households, the differences are subtle. Thus, for a given TAZ, the differences in impacts across incomes are not that great. There is, however, an unequal geographic distribution of wealth in the study region. Because of this, when we aggregate accessibility risk across TAZs, we see that accessibility risk rises slightly with

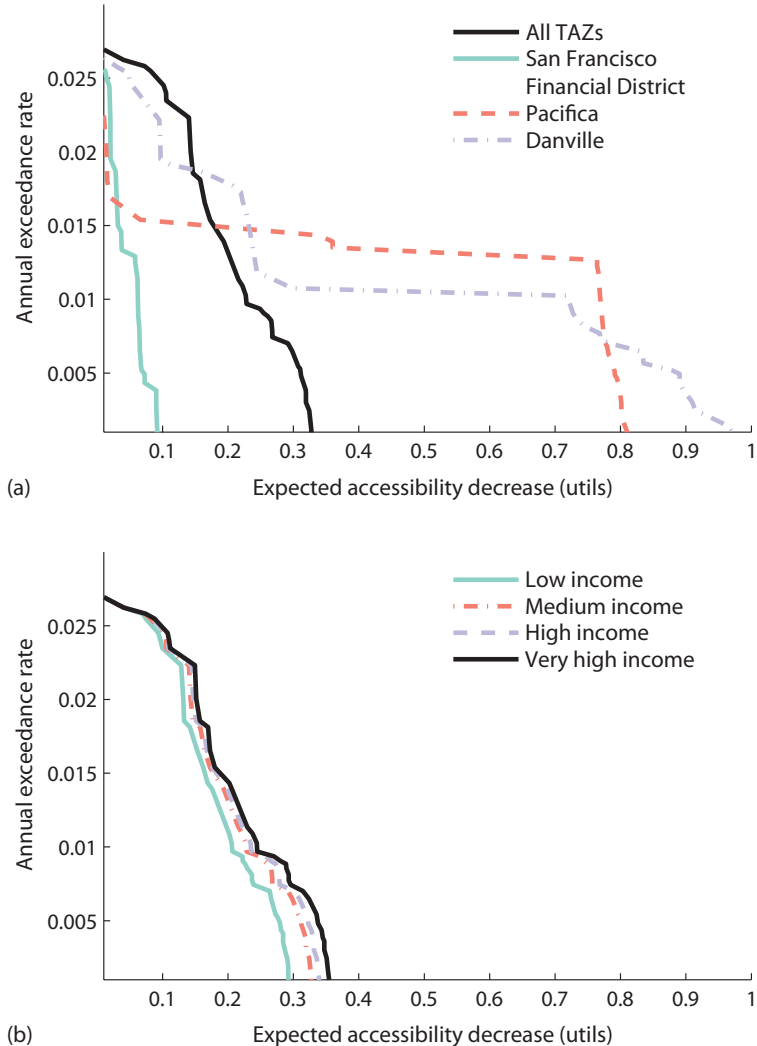


Figure 4. Accessibility annual loss exceedance curve with a comparison by (a) case study TAZs and average over all TAZs and (b) income class; all curves are for medium income households with fewer cars than workers.

increasing household income (Figure 4b).

Next, we consider TAZs indicated to have elevated risk. The San Francisco Peninsula is at risk of disruption from large magnitude San Andreas earthquakes, while the East Bay is at risk from slightly smaller but more frequent events on the Hayward Fault. Network simulations indicate that both Hayward and San Andreas earthquakes can cause accessibility problems for the East Bay. Figure 6 shows realizations of a magnitude 6.85 Hayward event and a magnitude 7.45 San Andreas event—both show high accessibility losses in the East Bay. In contrast, the main predicted accessibility losses in San Francisco correspond primarily to San Andreas events. Figures 6c and 6d provide one such example. Figures 6e and 6f show a lower magnitude event farther away from the main population centers: a magnitude 6.35 event in the Great Valley Pittsburg-Kirby Hills Fault. This shows how the more minor faults in the East Bay can contribute to that area's risk. The Figure 6 results are for one specific socio-economic group, but comparable results for the other groups show the same patterns.

Finally, we can examine the rates of loss exceedance (eq. 4), as shown in Figure 4. Recognizing that the impact

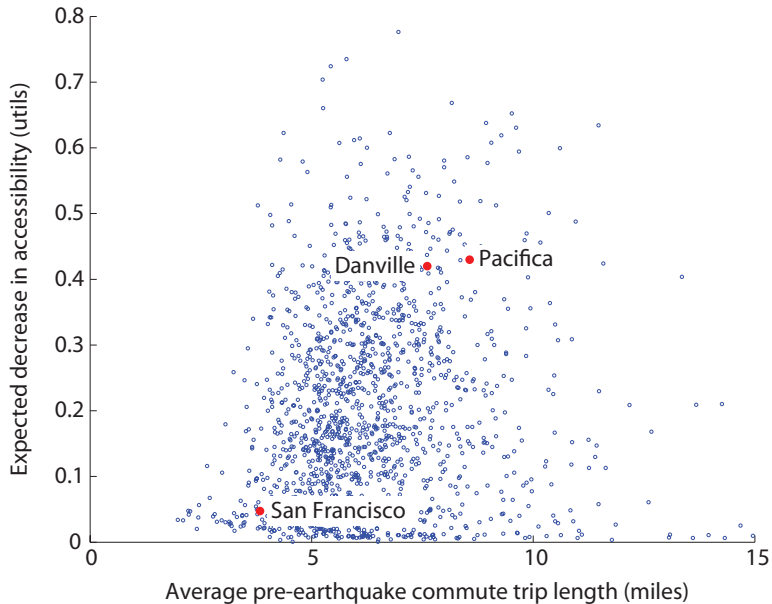


Figure 5. Average pre-earthquake trip length versus change in expected accessibility for all TAZs in the study region. Each dot represents data from one TAZ, and red dots highlight the data points for the three case study communities.

varies significantly by TAZ, as indicated by Figure 3, we also examine the accessibility loss exceedance curve for three communities: part of the San Francisco Financial District, Danville, and Pacifica. This part of the San Francisco Financial District represents an area with relatively low expected changes in accessibility, whereas Danville and Pacifica are at an elevated risk in almost all socio-economic groups (Figure 3). The general trends are corroborated by the loss exceedance curves for these three communities (Figure 4a shows results for medium income households with fewer cars than workers). The average middle-class person from Danville in a household with fewer cars than workers is expected to experience travel-related losses up to 1 *util* (or 75 minutes of extra travel time per day) after a rare earthquake. In contrast, a resident of San Francisco's Financial District has expected losses of only a tenth as much when considering the same exceedance rate. At annual rates of less than 0.01 (i.e., return periods greater than 100 years), Danville and Pacifica follow a similar general pattern that differs dramatically from that of San Francisco.

3.2. Analysis for San Francisco Financial District

Two factors may explain this San Francisco TAZ's lower accessibility losses relative to most other communities. First, it differs dramatically from many other TAZs in having a small percentage of trips made by car (38% versus an average of 85% across all TAZs). Households traveling by foot or bike are less influenced by network damage, because foot travel routes and travel times are assumed to not be affected by bridge damage and road congestion. Additionally, trips by foot and bike tend to be to destinations that are shorter distances away than trips made via other modes. Second, the times for trips to and from work are similar to that of other TAZs, and the average trip distance is only 7% lower than the average for all trips region-wide. So the trip times and lengths do not explain the differences in accessibility losses in this TAZ. The data thus suggests that a major cause for the low accessibility risk of this TAZ is the low dependence on cars for mobility.

3.3. Analysis for Pacifica

Pacifica is wedged between the Pacific Ocean to the west and the coastal mountains to the east. The main access road is historic California Highway 1, which has a number of older and seismically vulnerable bridges. There are no viable alternative routes to population centers via local roads. Most trips from Pacifica are taken by car (88%), and the average trip length is 108% longer than the region-wide average, so the Highway 1 vulnerability is particularly serious.

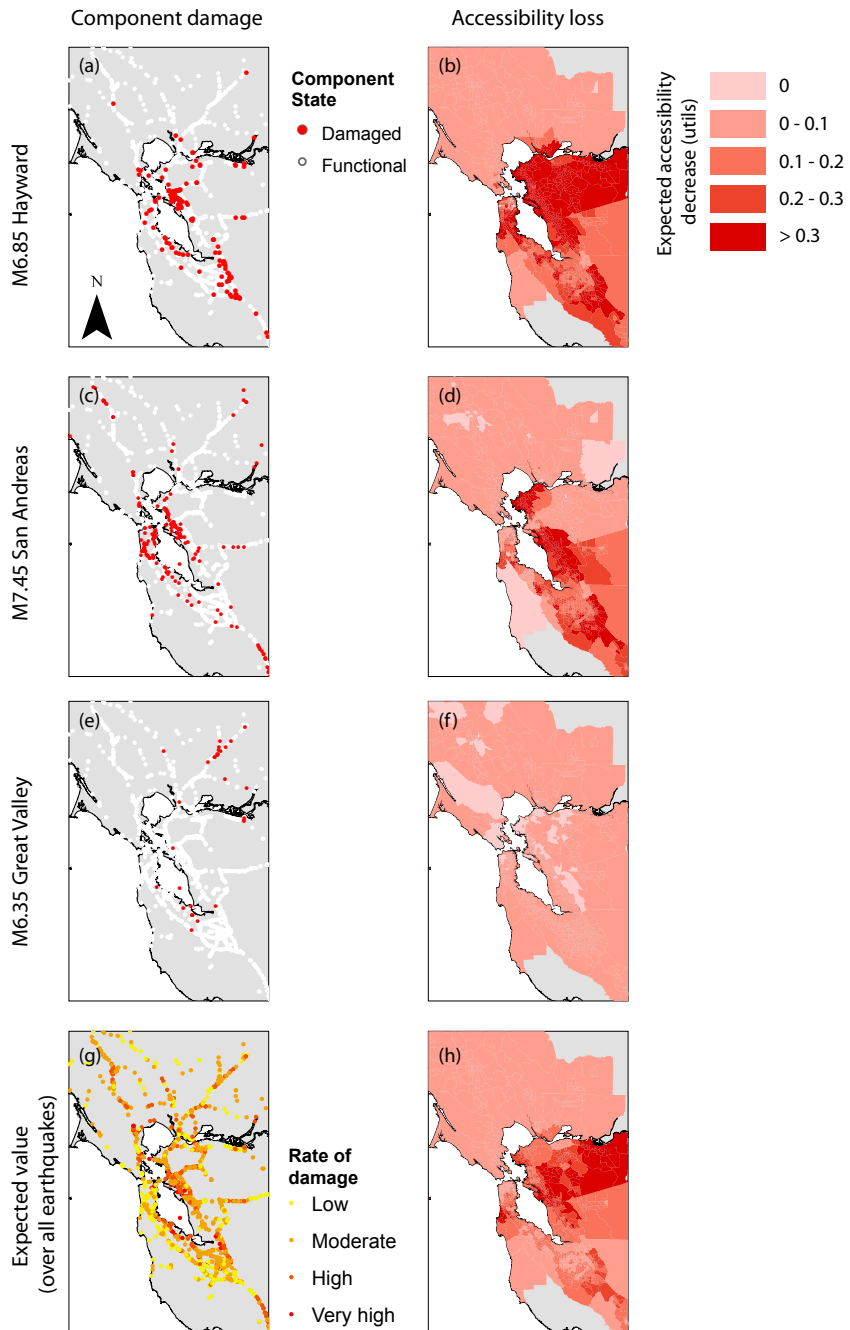


Figure 6. Bridge damage and corresponding accessibility losses by TAZ for medium income households with fewer cars than workers. The top three rows show results from specific events, while the bottom row has expected values calculated as a weighted average over all events.

273 As a comparison, consider Half Moon Bay, a community about 13 miles to the South (Figure 7). Half Moon Bay
 274 has significantly lower expected accessibility losses compared to Pacifica (0.11 *utils* for a middle income household
 275 with fewer cars than workers, versus 0.43 *utils* in Pacifica). While the seismic hazard for the two towns is similar, Half
 276 Moon Bay's population is about one third of Pacifica's, so there is less local demand for Highway 1's limited road
 277 capacity [43]. Perhaps more importantly, Half Moon Bay has a key alternative to California Highway 1: California

278 Highway 92, which links to the main highways of the peninsula. Since Pacifica is unusually reliant on one road with key vulnerabilities, it has an elevated risk for losses in accessibility.

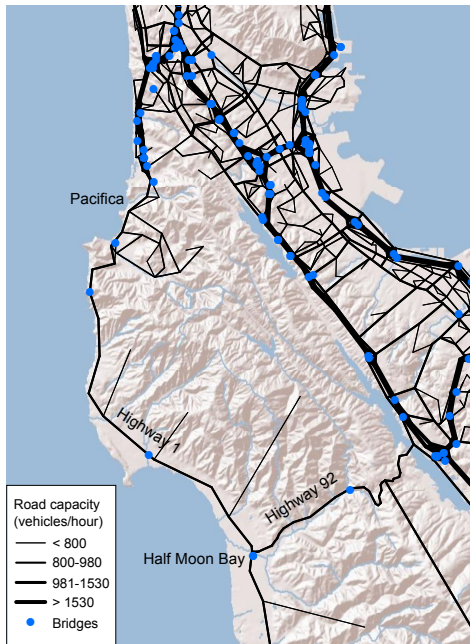


Figure 7. Roads providing access from Pacifica and Half Moon Bay.

279

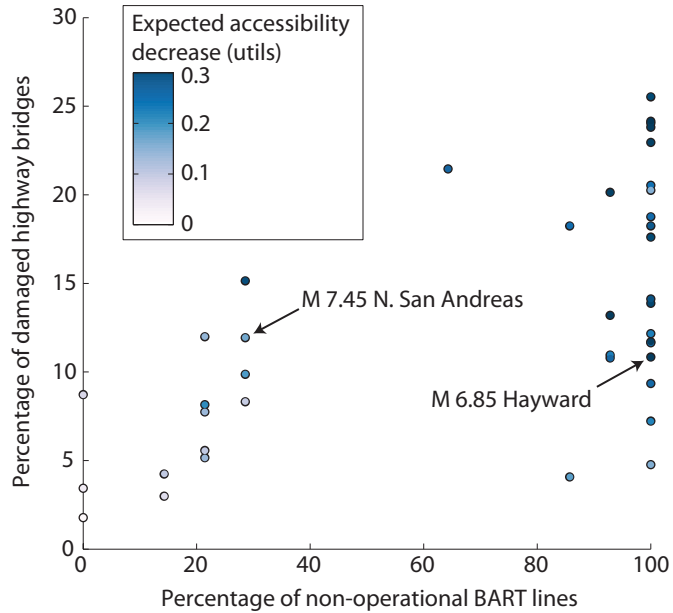
280 3.4. Analysis for Danville

281 Danville is a suburban community with many residents commuting large distances by car. The average length of
 282 a trip from Danville is 85% longer than the average over all trips in the study region, with a relatively high proportion
 283 of trips taking more than 60 minutes and traveling over 40 miles. These longer trips have more opportunities to
 284 be impacted by road closures, because more roads and bridges will be used to complete the trip. Moreover, many
 285 Danville trips are via highways, which increases the likelihood of crossing (damage prone) highway bridges.

286 Bridge damage is important for many regions, including Danville, because the percentage of car-based trips is
 287 high (85% of all trips from Danville, which is approximately average for all TAZs). For all three simulations shown in
 288 Figure 6, some bridges in the Oakland area are damaged and thus closed. In addition, in the first two simulations, there
 289 are closures to the north of Danville, which represents one of the two main travel routes from Danville. There are also
 290 scattered closed bridges to the west of Danville, a top travel corridor for people of Danville because of the workplace
 291 centers in San Francisco, Oakland, and San Jose (all to the west). As for transit, in the first two events, all BART
 292 lines are closed, so there are limited alternatives to the popular road routes. The result is that the residents of Danville
 293 have reduced access to their normal destinations after these events. Looking at the rate of bridge damage across all
 294 of the earthquake simulations in Figure 6g, we see that bridges in the Oakland area and to the north of Danville are
 295 particularly likely to be damaged. This suggests that Danville's proximity to vulnerable bridges contributes to its
 296 accessibility risk.

297 3.5. Impact of travel mode shifts and regional variations in travel mode patterns

298 Over all the simulated events, taking a weighted average by the annual occurrence rate of each event, we see a
 299 25% reduction in transit ridership after an earthquake. The heavy rail systems (BART and Caltrain) are not fully



operational in most of the forty simulated events (Table 2), and these have heavy ridership. The light rail systems (VTA and Muni) also suffer losses in many events (Table 2). Some of the pre-earthquake transit trips do not take place at all in the post-earthquake simulations, and some switch to other modes (car, foot and bike), causing small average increases in the number of trips taken by other modes. One exception to this trend is the M6.35 Great Valley earthquake illustrated in Figure 6e and 6f. In this event, there were no line closures on the four major transit systems listed in Table 2. There were, however, some bridge closures on the highways, resulting in a slight increase in transit ridership and in trips by foot.

In general, accessibility impact grows with increasing number of damaged transit lines, particularly in combination with high numbers of damaged bridges (Figure 8). Individual network simulations also suggest that transit is a key contributor to accessibility risk. For example, the M6.85 Hayward and the M7.45 Northern San Andreas Fault events from Figure 6 both have around 11% of bridges damaged. These events are labeled in Figure 8, which indicates that the Hayward event has significantly higher transit network damage and accessibility loss. The Northern San Andreas event had 10 of the 14 BART lines and all Muni lines operational, whereas the Hayward event had no BART lines and 5 of the 8 Muni lines operational (Caltrain and VTA were not operational in either simulation). Moreover, the differences in accessibility results could not have been predicted from simpler models focusing on bridge portfolio losses, because the percent of damaged bridges was about the same, and the San Andreas event actually corresponded to a greater increase in fixed-demand travel time when modeled using a much simpler traffic model.

Next, we examine the correlation between a community's walkability, as measured by the percentage of total trips made by that travel mode, and its expected decrease in accessibility. Figure 9 shows communities with a high

percentage of pre-earthquake trips on foot have a lower average decrease in accessibility. This result corroborates the specific example of the San Francisco Financial District discussed in Section 3.2. Furthermore, on average, the number of by-foot trips increases after the earthquake events where road congestion worsens. This model result is consistent with the observations after the 1995 Kobe earthquake, in which many commuters switched to walking and biking in the weeks after the earthquake [7]. This suggests that communities with greater walkability are also more resilient to earthquake-related accessibility risk.

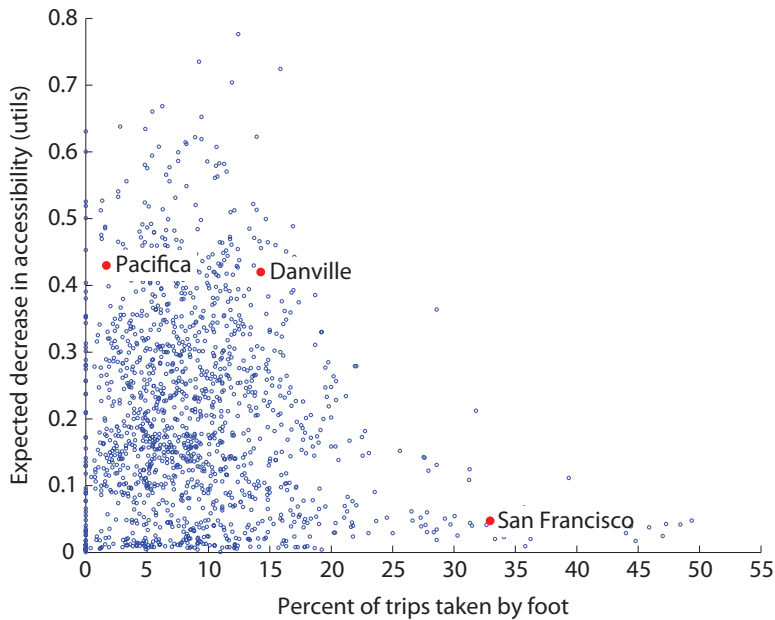


Figure 9. Percentage of pre-earthquake trips taken by foot versus expected decrease in accessibility among households with fewer cars than workers, for all TAZs in the study area. Each dot represents data from one TAZ, and red dots highlight the data points for the three case study communities.

4. Conclusions

We have shown how mode-destination accessibility can be used to link post-earthquake infrastructure damage to the impact on human welfare and enables identifying at-risk geographic and demographic groups in a region. Adopting this performance metric from the urban planning community, we have illustrated its use for seismic risk assessment and mitigation through a case study of the San Francisco Bay Area. For the case study, we considered a set of 40 hazard-consistent earthquake scenarios, ground-motion intensity maps, damage maps, and corresponding annual rates of occurrence. For each damage map, we performed a detailed activity-based travel model calculation that includes the road network, transit networks, walking and biking options, variable travel demand, and mode choice. We used this data and model to compute the mode-destination accessibility, a performance measure for each community and each socio-economic group (defined by income class and car ownership).

We saw stark differences in accessibility from location to location. We found that these geographic trends persisted across income classes and car ownership groups. Nonetheless, higher income households with more cars than workers had higher average accessibility losses than other socio-economic groups. One reason for this is the geographic clustering of these households in higher-risk areas. Another factor is that these households tend to take longer daily trips, thus crossing more roads and bridges and possibly increasing the likelihood of disruption. We also considered three specific communities that were predicted to have greatly differing experiences after a future earthquake, in order to understand the geographic and demographic reasons underlying these differences in risk.

This study considered the possibility that travel modes will shift after an earthquake, and communities that can more easily adjust are predicted to experience lower post-earthquake losses in accessibility. The results suggest that the walkability of a community, as measured by the percentage of pre-earthquake trips by foot, is closely linked to

345 reduced accessibility risk. We also found that in almost all of the simulated earthquake events, the transit system is
 346 predicted by this model to be severely impacted. The result is a reduced mode share for transit and increased trips by
 347 other modes (car, walking, and bike). Thus, this study suggests that neglecting to consider transit disruption can lead
 348 to a nonconservative estimate of seismic risk of transportation systems. The model shows, however, that when transit
 349 is not damaged—which is rare for this case study—ridership increases.

350 In conclusion, mode-destination accessibility offers important insights into the relationship between damage to
 351 physical infrastructure and impacts on human welfare. Using a detailed transportation network model, computationally
 352 efficient analysis strategies, and this refined measure of impact, we obtain new insights about users' risk, and
 353 obtain metrics that are usable by urban planners responsible for long-term management of transportation systems.
 354 This approach provides a foundation for future work in risk mitigation and policy to reduce the vulnerability of at-risk
 355 communities. It suggests that initiatives making communities more conducive for cycling and walking to work can
 356 increase resiliency to disasters. It also provides a method to quantify economic and societal benefits of upgrading
 357 various aspects of a region's transportation systems.

358 5. Acknowledgements

359 We thank Dave Ory at the Metropolitan Transportation Commission (MTC) and Tom Shantz and Loren Turner at
 360 Caltrans for motivating discussions and providing the case study data. The first author thanks the support of the NSF
 361 and Stanford Graduate Research Fellowships. This work was supported in part by the National Science Foundation
 362 under NSF grant number CMMI 0952402. Any opinions, findings and conclusions or recommendations expressed in
 363 this material are those of the authors and do not necessarily reflect the views of the National Science Foundation.

364 References

- 365 [1] L. Dueñas-Osorio, J. I. Craig, B. J. Goodno, Seismic response of critical interdependent networks, *Earthquake Engineering & Structural*
 366 *Dynamics* 36 (2) (2007) 285306. doi:10.1002/eqe.626.
- 367 [2] S. E. Chang, M. Shinohara, J. E. Moore, Probabilistic earthquake scenarios: Extending risk analysis methodologies to spatially distributed
 368 systems, *Earthquake Spectra* 16 (3) (2000) 557–572. doi:10.1193/1.1586127.
- 369 [3] R. C. Bolin, L. Stanford, *The Northridge earthquake: vulnerability and disaster*, Routledge, London; New York, 1998.
- 370 [4] The World Bank and the United Nations, *Natural hazards, unnatural disasters: the economics of effective prevention*, Tech. rep., The World
 371 Bank, Washington D.C. (2010).
- 372 [5] California. Dept. of Transportation. Post Earthquake Investigation Team, *Northridge earthquake, 17 January 1994: PEQIT report*, California
 373 Department of Transportation, Division of Structures, Sacramento, 1994.
- 374 [6] K. J. Tierney, Business Impacts of the Northridge Earthquake, *Journal of Contingencies and Crisis Management* 5 (2) (1997) 87–97.
 375 doi:10.1111/1468-5973.00040.
- 376 [7] P. Gordon, H. W. Richardson, B. Davis, Transport-related impacts of the Northridge earthquake, National Emergency Training Center, 1998.
- 377 [8] A. Kiremidjian, J. Moore, Y. Y. Fan, O. Yazlali, N. Basöz, M. Williams, Seismic risk assessment of transportation network systems, *Journal*
 378 *of Earthquake Engineering* 11 (3) (2007) 371–382. doi:10.1080/13632460701285277.
- 379 [9] N. Jayaram, J. W. Baker, Efficient sampling and data reduction techniques for probabilistic seismic lifeline risk assessment, *Earthquake*
 380 *Engineering & Structural Dynamics* 39 (10) (2010) 1109–1131. doi:10.1002/eqe.988.
- 381 [10] C. S. Oliveira, M. A. Ferreira, F. M. d. S., The concept of a disruption index: application to the overall impact of the July 9, 1998 Faial
 382 earthquake (Azores islands), *Bulletin of Earthquake Engineering* 10 (1) (2012) 7–25. doi:10.1007/s10518-011-9333-8.
- 383 [11] P. Bocchini, D. M. Frangopol, Restoration of bridge networks after an earthquake: Multicriteria intervention optimization, *Earthquake Spectra*
 384 28 (2) (2012) 426–455. doi:10.1193/1.4000019.
- 385 [12] F. Cavalieri, P. Franchin, P. Gehl, B. Khazai, Quantitative assessment of social losses based on physical damage and interaction with infra-
 386 structural systems, *Earthquake Engineering & Structural Dynamics* 41 (11) (2012) 1569–1589. doi:10.1002/eqe.2220.
- 387 [13] F. S. Chapin, *Urban land use planning*, University of Illinois Press, 1970.
- 388 [14] D. A. Niemeier, Accessibility: an evaluation using consumer welfare, *Transportation* 24 (4) (1997) 377396.
- 389 [15] K. T. Geurs, B. van Wee, Accessibility evaluation of land-use and transport strategies: review and research directions, *Journal of Transport*
 390 *Geography* 12 (2) (2004) 127–140. doi:10.1016/j.jtrangeo.2003.10.005.
- 391 [16] S. L. Handy, D. A. Niemeier, Measuring accessibility: an exploration of issues and alternatives, *Environment and Planning A* 29 (7) (1997)
 392 11751194.
- 393 [17] M. Miller, Seismic risk assessment of complex transportation networks, PhD thesis, Stanford University (2014).
- 394 [18] M. Miller, J. Baker, Ground-motion intensity and damage map selection for probabilistic infrastructure network risk assessment using opti-
 395 mization, in review (2014).
- 396 [19] R. Cervero, K.-L. Wu, Polycentrism, commuting, and residential location in the San Francisco Bay area, *Environment and Planning A* 29 (5)
 397 (1997) 865–886.
- 398 [20] Y. Han, R. A. Davidson, Probabilistic seismic hazard analysis for spatially distributed infrastructure, *Earthquake Engineering & Structural*
 399 *Dynamics* 41 (15) (2012) 2141–2158. doi:10.1002/eqe.2179.

- 400 [21] E. H. Field, T. H. Jordan, C. A. Cornell, OpenSHA: a developing community-modeling environment for seismic hazard analysis, *Seismological Research Letters* 74 (4) (2003) 406 – 419. doi:10.1785/gssrl.74.4.406.
- 401 [22] M. Shinozuka, Y. Murachi, X. Dong, Y. Zhou, M. J. Orlikowski, Effect of seismic retrofit of bridges on transportation networks, *Earthquake*
402 *Engineering and Engineering Vibration* 2 (2) (2003) 169–179. doi:10.1007/s11803-003-0001-0.
- 403 [23] E. H. Field, T. E. Dawson, K. R. Felzer, A. D. Frankel, V. Gupta, T. H. Jordan, T. Parsons, M. D. Petersen, R. S. Stein, R. J. Weldon, C. J.
404 Wills, Uniform California Earthquake Rupture Forecast, Version 2 (UCERF 2), *Bulletin of the Seismological Society of America* 99 (4)
405 (2009) 2053 –2107. doi:10.1785/0120080049.
- 406 [24] D. J. Wald, T. I. Allen, Topographic slope as a proxy for seismic site conditions and amplification, *Bulletin of the Seismological Society of*
407 *America* 97 (5) (2007) 1379–1395. doi:10.1785/0120060267.
- 408 [25] D. M. Boore, G. M. Atkinson, Ground-motion prediction equations for the average horizontal component of PGA, PGV, and 5%-damped
409 PSA at spectral periods between 0.01 s and 10.0 s, *Earthquake Spectra* 24 (1) (2008) 99–138.
- 410 [26] N. Jayaram, J. W. Baker, Correlation model for spatially distributed ground-motion intensities, *Earthquake Engineering & Structural Dynam-*
411 *ics* 38 (15) (2009) 1687–1708. doi:10.1002/eqe.922.
- 412 [27] N. Basöz, J. Mander, Enhancement of the highway transportation lifeline module in HAZUS, Tech. rep., Final Pre-Publication Draft (#7)
413 prepared for the National Institute of Building Sciences (NIBS) (1999).
- 414 [28] K. N. Ramanathan, Next generation seismic fragility curves for California bridges incorporating the evolution in seismic design philosophy,
415 PhD thesis, Georgia Institute of Technology (2012).
- 416 [29] S. Werner, C. Taylor, S. Cho, J. Lavoie, REDARS 2 methodology and software for seismic risk analysis of highway systems (technical
417 manual), Tech. rep., Seismic Systems & Engineering Analysis for MCEER, Oakland, CA (2006).
- 418 [30] Caltrans, Caltrans Seismic Design Criteria Version 1.7, Tech. Rep. SDC 1.7, California Department of Transportation, Sacramento, CA
419 (2013).
- 420 [31] Bechtel/HNTB Team, Design Criteria Volume I, Version 1.2, Tech. rep., San Francisco Bay Area Rapid Transit District, San Francisco Bay
421 Area Rapid Transit District Earthquake Safety Program (2008).
- 422 [32] N. Kurtz, J. Song, P. Gardoni, Time-varying seismic reliability analysis of representative US west coast bridge transportation networks, in:
423 G. Deodatis, B. R. Ellingwood, D. M. Frangopol (Eds.), *Safety, Reliability, Risk and Life-Cycle Performance of Structures and Infrastructures*,
424 CRC Press, 2014, pp. 655–662.
- 425 [33] J. Ghosh, K. Rokneddin, J. E. Padgett, L. Dueas-Osorio, Seismic reliability assessment of aging highway bridge networks with field instru-
426 mentation data and correlated failures. I: Methodology, *Earthquake Spectra* 30 (2) (2013) 795–817. doi:10.1193/040512EQS155M.
- 427 [34] K. Kockelman, Travel Behavior as Function of Accessibility, Land Use Mixing, and Land Use Balance: Evidence from San Francisco Bay
428 Area, *Transportation Research Record: Journal of the Transportation Research Board* 1607 (-1) (1997) 116–125. doi:10.3141/1607-16.
- 429 [35] P. Waddell, F. Nourzad, Incorporating nonmotorized mode and neighborhood accessibility in an integrated land use and transportation model
430 system, *Transportation Research Record: Journal of the Transportation Research Board* 1805 (-1) (2002) 119–127. doi:10.3141/1805-14.
- 431 [36] C. F. Manski, *Structural analysis of discrete data with econometric applications*, MIT Press, 1981.
- 432 [37] K. A. Small, H. S. Rosen, Applied welfare economics with discrete choice models, *Econometrica* 49 (1) (1981) 105–130.
433 doi:10.2307/1911129.
- 434 [38] D. Ory, Personal communication (2013).
- 435 [39] United States Department of Transportation, Revised departmental guidance: valuation of travel time in economic analysis, US Department
436 of Transportation, Washington, DC.
- 437 [40] G. Erhardt, P. Brinckerhoff, D. Ory, A. Sarvepalli, J. Freedman, J. Hood, B. Stabler, MTC's Travel Model One: applications of an activity-
438 based model in its first year, in: *Innovations in Travel Modeling 2012*, Tampa, Florida, 2012, p. 9.
- 439 [41] P. Waddell, UrbanSim: modeling urban development for land use, transportation, and environmental planning, *Journal of the American*
440 *Planning Association* 68 (3) (2002) 297–314. doi:10.1080/01944360208976274.
- 441 [42] W. Davidson, P. Vovsha, J. Freedman, R. Donnelly, CT-RAMP family of activity-based models, in: *Proceedings of the 33rd Australasian*
442 *Transport Research Forum (ATRF)*, Canberra, Australia, 2010, p. 15.
- 443 [43] U.S. Bureau of the Census, United States Census 2010, Tech. rep., U.S. Census Bureau, Washington D.C. (2010).